nature geoscience

ARTICLES

https://doi.org/10.1038/s41561-018-0081-0

Global niche of marine anaerobic metabolisms expanded by particle microenvironments

Daniele Bianchi[1,5]*, Thomas S. Weber[2,5], Rainer Kiko[3] and Curtis Deutsch[4]

In ocean waters, anaerobic microbial respiration should be confined to the anoxic waters found in coastal regions and tropical oxygen minimum zones, where it is energetically favourable. However, recent molecular and geochemical evidence has pointed to a much broader distribution of denitrifying and sulfate-reducing microbes. Anaerobic metabolisms are thought to thrive in microenvironments that develop inside sinking organic aggregates, but the global distribution and geochemical significance of these microenvironments is poorly understood. Here, we develop a new size-resolved particle model to predict anaerobic respiration from aggregate properties and seawater chemistry. Constrained by observations of the size spectrum of sinking particles, the model predicts that denitrification and sulfate reduction can be sustained throughout vast, hypoxic expanses of the ocean, and could explain the trace metal enrichment observed in particles due to sulfide precipitation. Globally, the expansion of the anaerobic niche due to particle microenvironments doubles the rate of water column denitrification compared with estimates based on anoxic zones alone, and changes the sensitivity of the marine nitrogen cycle to deoxygenation in a warming climate.

Throughout the well-oxygenated ocean interior, microbes use oxygen (O_2) to respire and derive energy from sinking organic matter. In anoxic waters, where O_2 falls below nanomolar levels[1], specialized microbes dominate the community and respire using a sequence of alternative oxidants, in order of their free energy yield, as commonly observed in sediments[2]. Of the oxidants that are abundant in seawater, nitrate (NO_3^-) yields the most energy after O_2, followed by sulfate (SO_4^{2-}). It follows that, outside sediments, denitrifying metabolisms (which reduce NO_3^- to dinitrogen gas N_2) should be confined to anoxic waters of coastal regions and tropical oxygen minimum zones (OMZs) and SO_4^{2-} reducers should lack a niche in the open ocean where O_2 and NO_3^- exhaustion never overlap[3,4].

Recently, multiple lines of evidence have challenged this traditional view of microbial respiration in the ocean. Microbial lineages with the ability to reduce nitrogen (N) have been observed in oxygenated waters[5,6], and nitrogen-based respiration has been measured outside anoxic waters[7–9]. Molecular evidence further indicates that sulfur-based metabolism is active within each of the ocean's three major OMZs[10–12] in the presence of abundant nitrate, and potentially over vast oxygenated regions[13].

The occurrence of anaerobic metabolisms outside anoxic regions might be explained by the formation of microenvironments inside sinking organic aggregates, where concentrated respiration results in local O_2 exhaustion[14,15]. Anoxic microenvironments have been observed within millimetre-scale marine aggregates[14,15], and appear to support both denitrification[7,8,16,17] and sulfate reduction[18]. Hydrogen sulfide (H_2S) liberated in microenvironments could drive the precipitation of chalcophile metals as insoluble complexes, which might explain the dissolved deficits and particulate enrichments of trace metals observed in hypoxic regions (where oxygen concentrations $[O_2]$ are $<60\,\mu M$)[19,20]. Despite this wide range of observations, the conditions that drive the formation of microenvironments and their integrated effect on global biogeochemical cycles remain highly uncertain.

Particle size spectrum and microenvironment model

To close these gaps, we developed a new size-resolved model of sinking organic particles that explicitly simulates the formation of anoxic microenvironments and predicts the rates of anaerobic metabolism that they harbour (Fig. 1). Particle transformations in the ocean depend on the complex interaction of physical, chemical and biological processes, many of which are still being uncovered[21–24]. Our model employs simplified, data-constrained parameterizations of these transformations, and takes a first step towards explicitly coupling particle-scale biogeochemistry to seawater chemistry.

A power-law size spectrum of particles is produced in the surface euphotic zone of the model and evolves over depth due to differential settling[25], disaggregation[23] and remineralization[24] (Methods, Fig. 1a). The model then tracks the size, particulate organic carbon (POC) mass and number density of particles in hundreds of classes through the water column. At the particle scale, remineralization is represented by first-order respiration of POC by oxidants (O_2, NO_3^-, SO_4^{2-}) diffusing in from the surrounding seawater (Fig. 1b, Methods). Oxidants are utilized in a stepwise manner in order of their free energy yield[2], and their internal distribution inside each particle is solved (Fig. 1c) based on a spherical diffusion-reaction balance, assuming diffusive equilibrium with the environment (see Supplementary Information). If the diffusive supply of O_2 cannot meet its demand by respiration, an anoxic microenvironment forms (Fig. 1b,c), in which respiration proceeds using NO_3^-. Should denitrification exhaust NO_3^-, a second, sulfate-reducing zone forms in the particle core (Fig. 1b,c). In both microenvironments, respiration rates are slowed in proportion to the free energy yield of each anaerobic pathway relative to aerobic respiration. This results in a small (~1%) slowdown during denitrification, but an almost tenfold

---

[1]Department of Atmospheric and Oceanic Sciences, University of California Los Angeles, Los Angeles, CA, USA. [2]Department of Earth and Environmental Sciences, University of Rochester, Rochester, NY, USA. [3]GEOMAR Helmholtz Centre for Ocean Research Kiel, Kiel, Germany. [4]School of Oceanography, University of Washington, Seattle, WA, USA. [5]These authors contributed equally: Daniele Bianchi and Thomas S. Weber. *e-mail: dbianchi@atmos.ucla.edu

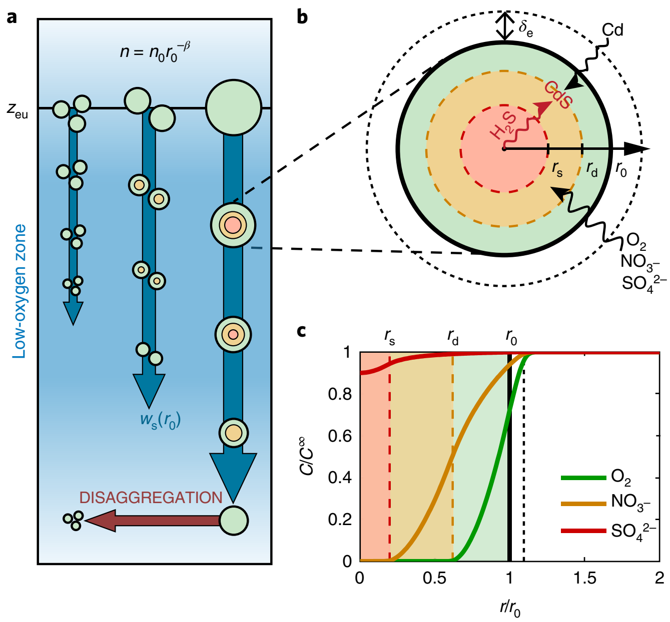

Fig. 1 | Particle size spectrum and microenvironment model schematic. **a**, The model simulates a size spectrum of particles leaving the euphotic zone (z_{eu}), and evolving over depth due to size-dependent sinking rates (w_s), remineralization and disaggregation. **b**, Schematic of an individual particle surrounded by a diffusive boundary layer δ_e (dashed black line), with colours indicating redox microenvironments in which respiration is fuelled sequentially by O_2 (green), NO_3^- (orange) and SO_4^{2-} (red). Hypoxic to anoxic conditions favour anaerobic respiration within large particles, and precipitation of Cd as CdS is simulated in particles undergoing SO_4^{2-} reduction. **c**, Oxidant concentrations (C) normalized to seawater concentrations (C^∞) inside a particle of radius $r_0 = 1$ mm sinking through a water column with $[O_2] = 50\,\mu$M and $[NO_3^-] = 10\,\mu$M. Sulfate depletion relative to seawater is multiplied by 10 times for clarity. Coloured shading and vertical lines represent zones and boundaries as in panel **b**.

slowdown during SO_4^{2-} reduction, consistent with more complex mechanistic models of microbial metabolism[26].

Particle properties that strongly influence the onset of anaerobic respiration include their size, internal diffusivity, volumetric POC content and remineralization rates (Supplementary Information). We therefore simulated a range of particle sizes representative of the open ocean (10 µm–5 mm diameters)[27,28], and parameterized the model using measured particle diffusivities[29], a compilation of observed POC versus size relationships (Supplementary Fig. 1a) and depth-varying respiration rates as observed by particle incubators in the low-latitude ocean[24] (Supplementary Fig. 1b).

Model case studies

We applied our model in two regions where recent observations indicate redox cycles that cannot be explained by seawater chemistry alone[6,9,11,20]: the Eastern Tropical South Pacific (ETSP, Fig. 2a–c, Supplementary Fig. 2a,b) and the Mauritanian upwelling zone in the North Atlantic Ocean (Fig. 2d–f, Supplementary Fig. 2c,d). In each region, observed O_2 and NO_3^- profiles were used as chemical boundary conditions for the diffusion-reaction model (Fig. 2a,d), and poorly-constrained rates of particle disaggregation were optimized to reproduce the size spectra observed by Underwater Vision Profiler 5 (UVP5)[30] and realistic flux profiles[31] (Methods, Supplementary Figs. 2–4). This ensures that size-dependent microenvironment processes are integrated across a realistic particle size distribution (PSD, Fig. 2a,d) to estimate their contribution to water column respiration.

In the ETSP, a thick OMZ is observed in the water column between ~150–600 m depth (Fig. 2a), with $[O_2]$ in the suboxic range (<5 µM). Our model predicts that small particles (diameter < 100 µm) only develop anoxic interiors as they sink through this suboxic layer, whereas larger particles can sustain anaerobic microenvironments in the hypoxic waters above and below it (Fig. 2b). This expands the niche of denitrifiers vertically into the upper and lower oxyclines, as previously suggested[32], and allows denitrification to fuel >1% of total particle respiration in waters as deep as 1,000 m (Fig. 2c), where genomic evidence also indicates NO_3^- reduction on particles[6]. Furthermore, sulfate-reducing zones develop in large aggregates (>0.5 mm) throughout the OMZ, and particularly within the upper oxycline between 100–300 m depth (Fig. 2b) where respiration is fastest (Supplementary Fig. 1b) and there is less NO_3^- to fuel denitrification (Fig. 2b). Integrated across the size spectrum, 25–40% of the total particle volume harbours SO_4^{2-} reduction in this depth interval (Fig. 2c). However, because SO_4^{2-} reduction decomposes POC approximately tenfold slower than aerobic respiration, it contributes only ~5% of total carbon remineralization in the anoxic zone (Fig. 2c)—within the range suggested by incubation experiments from anoxic waters off the coast of Chile[11], and easily accommodated by isotopic constraints[33]. As a result of this respiration slowdown, particle fluxes attenuate less rapidly with depth compared with oxygenated waters (Supplementary Fig. 3d), in agreement with observations from anoxic regions[34].

The water column of the Mauritanian upwelling is better oxygenated than the ETSP, but $[O_2]$ drops to hypoxic levels in the thermocline between 100–600 m (Fig. 2d). Here, our model predicts that only large millimetre-sized aggregates develop anoxic microenvironments, but the relatively low $[NO_3^-]$ in the Atlantic thermocline cannot meet the residual oxidant demand in these particles, which rapidly progress to sulfidic conditions (Fig. 2e). Integrated across the size spectrum, ~10% of the particle volume sustains respiration by SO_4^{2-} reduction in the upper oxycline, compared with 5% by denitrification (Fig. 2f).

Our assumption that denitrification proceeds at a similar rate to aerobic respiration (due to their comparable free energy yields) does not account for potential slowing due to particle colonization or biochemical limitations. However, our results are relatively insensitive to this factor: halving the C-specific respiration rate during denitrification reduces water column denitrification and sulfate reduction rates by less than 20% in our case study sites (Supplementary Fig. 5).

Trace metal precipitation

Our model prediction of sulfidic particles in the Mauritanian upwelling zone is consistent with the hypothesis that elevated particulate cadmium (Cd) relative to phosphorus (P) observed in the region reflects Cd precipitation as sulfide complexes within microenvironments[20]. To test this hypothesis quantitatively, we extended our microenvironment model to simulate CdS accumulation (Fig. 1b). In particles undergoing active SO_4^{2-} reduction we assume that H_2S is abundant enough to precipitate all Cd diffusing into the particle, which is computed from the observed Cd concentration profile (see Methods), and Cd released internally during organic matter remineralization. When SO_4^- reduction ceases in well-oxygenated waters, the accumulated CdS is assumed to dissolve at a first-order rate.

We used an optimization method to test whether our model of sulfide precipitation can explain the particulate Cd:P ratios observed in the Mauritanian upwelling zone, without violating observational constraints on model parameters (Methods, Supplementary Table 4). With only minor adjustment from the default parameter values used in previous simulations (Fig. 2), our model can accurately reproduce the broad characteristics of observed particle profiles from the region (Fig. 3, Supplementary Fig. 6). As particulate organic P (proportional to POC) remineralizes and CdS accumulates

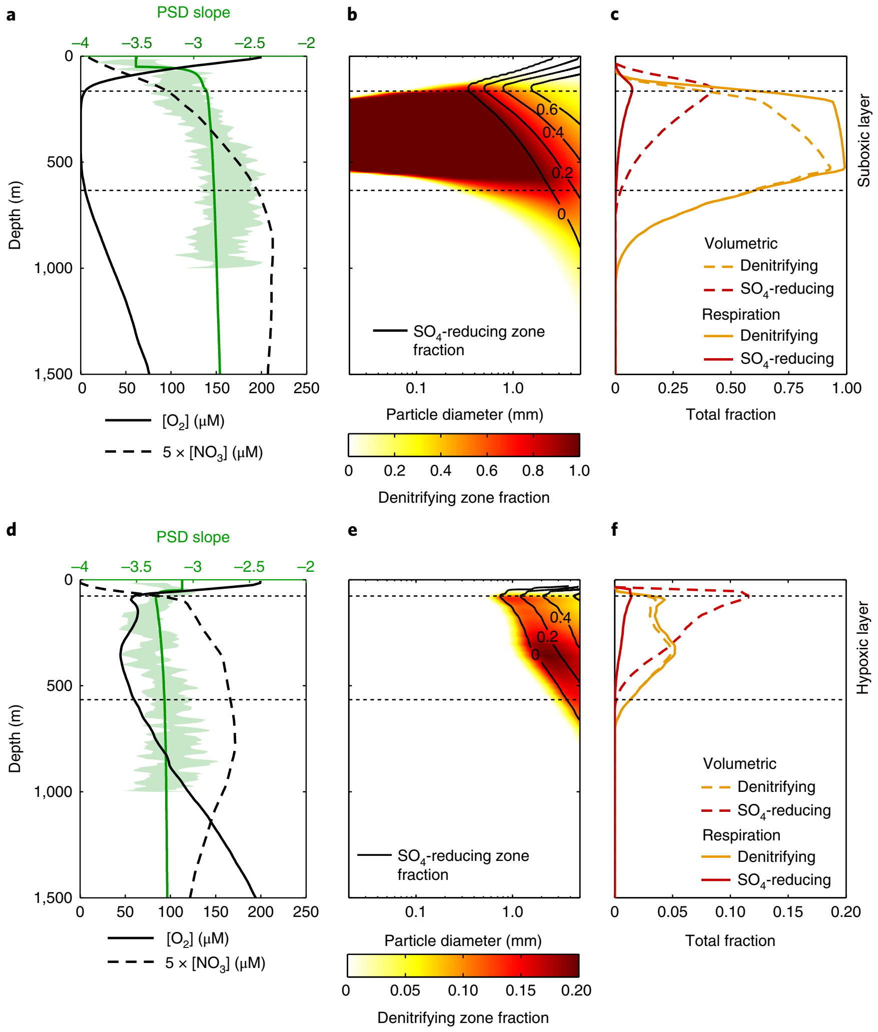

Fig. 2 | Predicted microenvironment distributions at two sites in the tropical ocean. a–c, ETSP. **d–f**, Mauritanian upwelling. **a**,**d**, Observed O_2 (solid black line) and NO_3^- (dashed black line) profiles, and the slope of the PSD from the model (green line) and from underwater vision profilers (green shading, 90% confidence intervals). **b**,**e**, Fraction of particle volume where respiration is fuelled by denitrification (background colours) and SO_4^{2-} reduction (black contours). **c**,**f**, Total fraction of particle volume (dashed lines) and respiration (solid lines) associated with denitrifying and SO_4^{2-}-reducing metabolisms, integrated across all particle size classes.

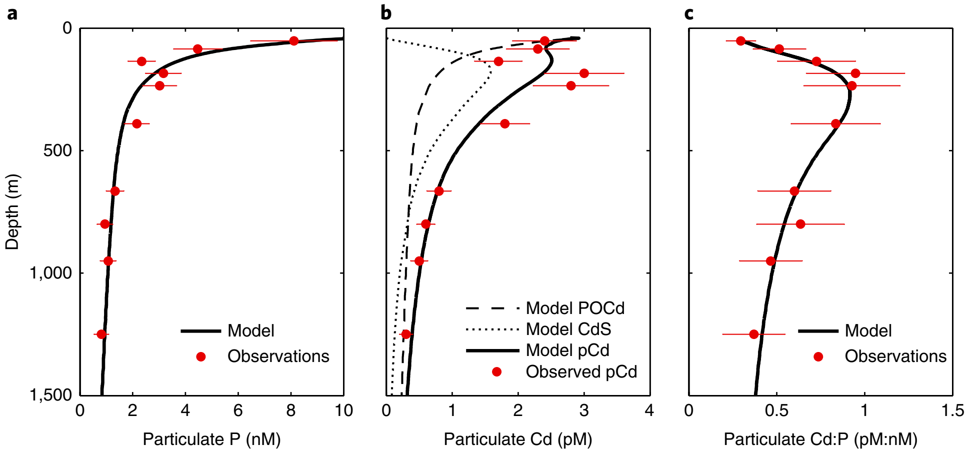

Fig. 3 | Microenvironment-driven accumulation of trace metals in the tropical North Atlantic. Simulated particle properties (integrated over the size spectrum) from optimized microenvironment model (thick black lines) compared with observations (red dots, with 2σ uncertainty) from the Mauritanian upwelling zone. **a**, Particulate organic phosphorous, related to POC using Redfield stoichiometry (106 C:1 P). Observations are from ref. [20]. **b**, Particulate Cd (pCd), including the simulated contribution of particulate organic Cd (POCd) and CdS. **c**, The pCd:P ratio.

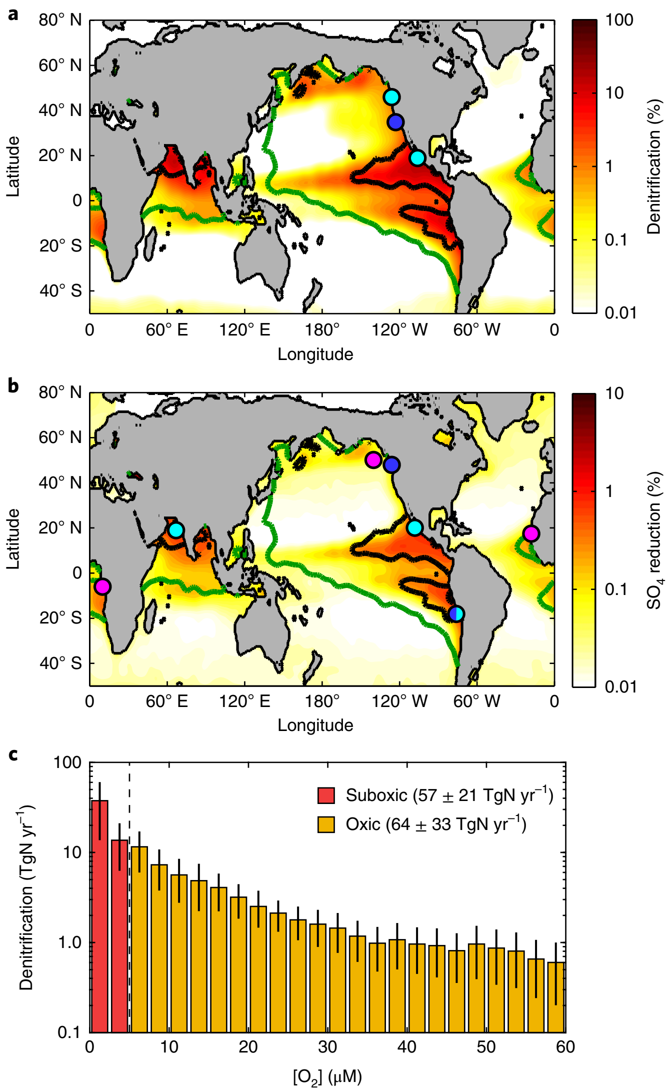

Fig. 4 | Expanded niche of anaerobic metabolism in the ocean. a,**b**, Predicted contribution of denitrification (**a**) and SO_4^{2-} reduction (**b**) to depth-integrated POC respiration. Green and black contours enclose hypoxic and suboxic regions, respectively. Based on seawater chemistry alone, anaerobic respiration should only be expected within the black contour. Coloured dots indicate direct (blue)[7-9,11], molecular (cyan)[5,6,10-12] and trace metal (magenta)[19,20] evidence that suggests denitrification is occurring in the presence of O_2 (**a**) and SO_4^{2-} reduction in the presence of NO_3^- (**b**). Maps average 24 simulations sampling observed ranges for uncertain parameters (Supplementary Table 4). **c**, Water column denitrification rates integrated over volumes with a given $[O_2]$, estimated by combining the microenvironment model with satellite estimates of POC export (Methods). Bars and error bars represent the mean and s.d., respectively, obtained from combining 24 model parameter sets and 9 POC export estimates (216 different estimates in total).

in the hypoxic layer (Fig. 3a,b), particulate Cd:P reaches a pronounced peak at ~300 m (Fig. 3c). In deeper waters, CdS dissolves from re-oxygenating particles, and Cd:P gradually declines back towards the ratio assumed for organic matter itself.

The close agreement between our model results and observations suggests that CdS precipitation is a plausible explanation for particulate Cd enrichment in this region[20], although other hypotheses cannot be ruled out. Similar elevated Cd:P ratios were recently observed extending from the ETSP OMZ[35], but have been attributed to trace metal enrichment of prokaryotic communities living in anaerobic waters[35] and scavenging by Fe oxyhydroxides[36]. Further modelling work that leverages seawater and particulate chemistry constraints, including element partitioning between different particle size classes[36], might help to distinguish between these competing hypotheses.

Global distribution of microenvironments

To assess the global distribution and biogeochemical role of anoxic microenvironments, we applied the model to each O_2 and NO_3^- profile in the World Ocean Atlas climatology[3]. We adopted a globally uniform surface particle spectrum distribution based on analysis of UVP5 measurements[37] (Supplementary Fig. 7), and tested a broad swathe of parameter values in cases where uncertainty ranges are well established from observations (Methods, Supplementary Table 4).

Our global simulation predicts that the three major OMZs in the Tropical Pacific and Arabian Sea are the only regions where denitrification contributes >10% of total depth-integrated respiration, but microenvironments support appreciable denitrification throughout large hypoxic regions of the tropics, and the subtropical and subarctic North Pacific (Fig. 4a). In the model, denitrification contributes >1% of POC decomposition in 3–6% of the global water column (4.5–9 × 10^7 km^3, where the range reflects uncertainty in model parameters), representing a ~100-fold geographical range expansion relative to the volume of permanently suboxic waters (~5 × $10^5$$km^3$). Sulfate reduction contributes approximately 1% of depth-integrated POC respiration in OMZ regions, and is sustained at lower levels (~0.1%) throughout the tropics, coastal zones and the subarctic North Pacific (Fig. 4b). These ranges encompass locations where molecular evidence, direct observations and trace metal distributions suggest denitrification in the presence of dissolved O_2 and SO_4^{2-} reduction in the presence of O_2 and NO_3^- [5,6,8,10-12,18] (Fig. 4a,b). Our model shows that all these disparate observations could be explained by widespread particle microenvironments, which expand the niche of anaerobic metabolisms far beyond the limits implied by seawater chemistry.

We estimated absolute rates of particle-associated denitrification in the water column by combining our model results with satellite estimates of organic carbon export from the euphotic zone[31], which determines the total carbon available for respiration through the water column (Methods). After propagating uncertainty in model parameters and satellite export estimates, this calculation yields an integrated water column denitrification rate of ~57 ± 21 TgN yr^{-1} within the OMZs, which is similar to previous estimates based on excess N_2 gas measurements[38], nitrate deficits[39] and particle flux within OMZs[40]. However, we find that particle-associated denitrification outside of suboxic waters contributes a similar N loss rate (64 ± 33 TgN yr^{-1}) when integrated across the expansive hypoxic regions that sustain anaerobic microenvironments (Fig. 4c, Supplementary Fig. 8). When combined, this yields a global water column denitrification rate of 121 ± 54 TgN yr^{-1}, approximately double that of current estimates based on suboxic zones alone.

Large-scale precipitation rates of chalcophile trace metals can also be predicted in our global model, based on the abundance of sulfidic microenvironments and the distribution of trace metals, which we mapped using their strong statistical relationship to other nutrients (Methods). If microenvironments are indeed responsible for scavenging trace metals, they could contribute to the removal of up to 1.4 ± 0.8 Gmol yr^{-1} of Cd and 9.7 ± 4.2 Gmol yr^{-1} of zinc (Zn) from hypoxic thermocline waters and their delivery to deeper layers—significant rates compared with the thermocline inventories of those metals (~100 Gmol and ~800 Gmol respectively, between 0–1,000 m). This process might contribute to the slight decoupling of Cd from macronutrient cycles[41], and explain Zn stress of diatoms in upwelling zones[42].

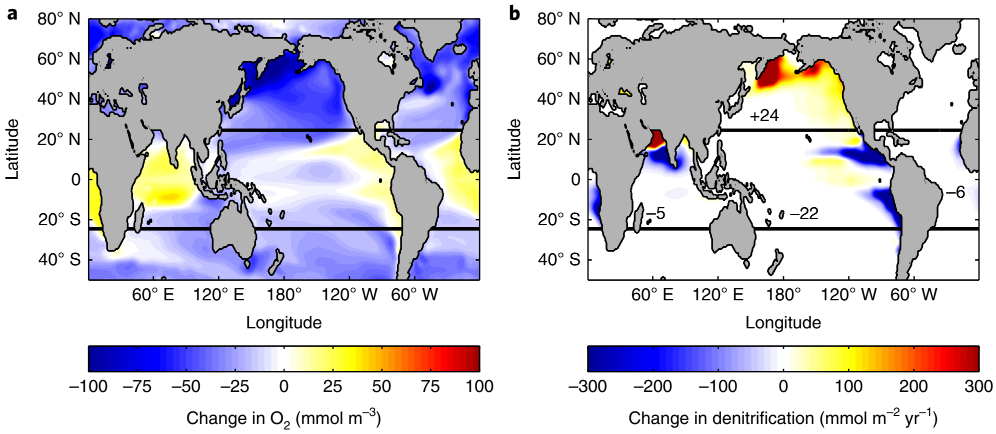

Fig. 5 | Sensitivity of particle denitrification to climate-forced oxygen trends. a, Mean O_2 change between 1900 and 2100 in the upper 1,000 m, averaged across five CMIP5 simulations (Supplementary Table 5) under the high-emission RCP8.5 scenario. **b**, Change in vertically integrated denitrification predicted by the particle model, forced by the CMIP5 O_2 change. Regional integrals (TgN yr^{-1}) in the tropics and subarctic North Pacific are annotated.

Implications for the global N cycle

The prevalence of denitrifying microenvironments implied by our model would change the traditional view of marine N loss inferred from geochemical tracers. The mean-ocean isotopic composition of NO_3^- suggests that 1.3–3 times more N is removed by benthic denitrification in anoxic sediments, where isotopes are not fractionated, than in the suboxic water column where isotopes are strongly fractionated[43–45]. The upwards revision of water column rates predicted here (Fig. 4c) may thus require a corresponding increase in benthic denitrification. In turn, this would imply an imbalance of the ocean N budget, unless the increased fixed N losses are balanced by higher N fixation rates than are currently assumed. This possibility is consistent with upwards revisions of global N fixation estimates[46], reflecting widespread activity of cyanobacterial diazotrophs or, potentially, heterotrophic diazotrophs[47]. Alternatively, the increase in water column denitrification could be accommodated by a different fractionation effect for particle-bound denitrification in the oxygenated ocean. Denitrification outside OMZ waters is confined to very large particles that completely deplete nitrate diffusing in from seawater, as evidenced by their rapid progression to SO_4^{2-}reduction (Fig. 2b,e). This localized depletion should result in weaker effective isotope fractionation than is expected for water column denitrification. Some of the non-fractionating denitrification previously assumed to occur in sediments might therefore occur in the hypoxic water column instead, changing the relative contribution of these environments to observed fixed N deficits.

The broad distribution of particle-bound denitrification would also imply a more complex sensitivity of water column denitrification to climate-driven changes in O_2 than previously recognized. The Earth system models compiled by the Fifth Climate Model Intercomparison Project (CMIP5) predict that anthropogenic global warming will result in a decline of the mean ocean O_2 content due to reduced solubility and enhanced stratification of the upper ocean[48]. Counter to the global trend, the tropical thermocline oxygenates over the same period in these models (Fig. 5a), probably due to weakened upwelling as the trade winds slacken in a warming climate[49].

To illustrate the response of particle-bound denitrification to these changes, we repeated our global microenvironment calculations while imposing ensemble-mean $[O_2]$ changes between 1900 and 2100 from the CMIP5 high-emission scenario (Supplementary Table 5) on the observed distribution (Methods). We find that tropical oxygenation reduces denitrification rates in low-latitude upwelling zones by 34 TgN yr^{-1}, whereas the broader deoxygenation trend expands hypoxic conditions in the subarctic North Pacific, increasing particle-bound denitrification by 24 TgN yr^{-1}. These results imply that climate-forced changes in ocean $[O_2]$ could drive a major shift of denitrification from low to high latitudes in the Pacific Ocean, with important implications for N limitation of primary production.

The large-scale distribution and climate sensitivity of microenvironment respiration predicted by our model (Figs. 4 and 5) is consistent with a range of data constraints, but requires further confirmation by direct observations. Efforts to assess the distribution of microbes with anaerobic capability, their association with particles and the relative efficiency of aerobic and anaerobic metabolism will provide valuable new constraints, and stand to benefit from application of modern molecular and biogeochemical approaches[11,17] at the scale of individual aggregates[16]. Future modelling work should target the broad signatures that widespread particle-bound denitrification, sulfate reduction and trace metal scavenging would leave on seawater geochemistry, which will provide important diagnostic constraints on these process rates.

Methods

Methods, including statements of data availability and any associated accession codes and references, are available at https://doi.org/10.1038/s41561-018-0081-0.

Received: 30 August 2017; Accepted: 9 February 2018;

References

1. Thamdrup, B., Dalsgaard, T. & Peter Revsbech, N. Widespread functional anoxia in the oxygen minimum zone of the eastern South Pacific. *Deep Sea Res. Pt I* **65**, 36–45 (2012).
2. Froelich, P. N. et al. Early oxidation of organic matter in pelagic sediments of the eastern equatorial Atlantic: suboxic diagenesis. *Geochim. Cosmochim. Acta* **43**, 1075–1090 (1979).
3. Garcia, H. E. et al. *World Ocean Atlas 2009, Volume 4: Nutrients (Phosphate, Nitrate, and Silicate)* NOAA Atlas NESDIS 71 (U.S. Government Printing Office, Washington, DC, 2010).
4. Ulloa, O., Canfield, D. E., DeLong, E. F., Letelier, R. M. & Stewart, F. J. Microbial oceanography of anoxic oxygen minimum zones. *Proc. Natl Acad. Sci. USA* **109**, 15996–16003 (2012).
5. Smith, M. W., Allen, L. Z., Allen, A. E., Herfort, L. & Simon, H. M. Contrasting genomic properties of free-living and particle-attached microbial assemblages within a coastal ecosystem. *Front. Microbiol.* **4**, 120 (2013).

6. Ganesh, S., Parris, D. J., DeLong, E. F. & Stewart, F. J. Metagenomic analysis of size-fractionated picoplankton in a marine oxygen minimum zone. *ISME J.* **8**, 187–211 (2014).
7. Michotey, V. & Bonin, P. Evidence for anaerobic bacterial processes in the water column: denitrification and dissimilatory nitrate ammonification in the northwestern Mediterranean Sea. *Mar. Ecol. Progress. Ser.* **160**, 47–56 (1997).
8. Wolgast, D., Carlucci, A. & Bauer, J. Nitrate respiration associated with detrital aggregates in aerobic bottom waters of the abyssal NE Pacific. *Deep Sea Res. Pt II* **45**, 881–892 (1998).
9. Kalvelage, T. et al. Oxygen sensitivity of anammox and coupled N-cycle processes in oxygen minimum zones. *PLoS ONE* **6**, e29299 (2011).
10. Fuchs, B. M., Woebken, D., Zubkov, M. V., Burkill, P. & Amann, R. Molecular identification of picoplankton populations in contrasting waters of the Arabian Sea. *Aquat. Microb. Ecol.* **39**, 145–157 (2005).
11. Canfield, D. E. et al. A cryptic sulfur cycle in oxygen-minimum–zone waters off the Chilean coast. *Science* **330**, 1375–1378 (2010).
12. Carolan, M. & Beman, J. M. Transcriptomic evidence for microbial sulfur cycling in the eastern tropical North Pacific oxygen minimum zone. *Front. Microbiol.* **6**, 334 (2015).
13. Swan, B. K. et al. Potential for chemolithoautotrophy among ubiquitous bacteria lineages in the dark ocean. *Science* **333**, 1296–1300 (2011).
14. Alldredge, A. L. & Cohen, Y. Can microscale chemical patches persist in the sea? Microelectrode study of marine snow, fecal pellets. *Science* **235**, 689–691 (1987).
15. Ploug, H. & Buchholz, B. Anoxic aggregates an ephemeral phenomenon in the ocean. *Aquat. Microb. Ecol.* **13**, 285–294 (1997).
16. Klawonn, I., Bonaglia, S., Brüchert, V. & Ploug, H. Aerobic and anaerobic nitrogen transformation processes in N2-fixing cyanobacterial aggregates. *ISME J.* **9**, 1456–1466 (2015).
17. Ganesh, S. et al. Size-fraction partitioning of community gene transcription and nitrogen metabolism in a marine oxygen minimum zone. *ISME J.* **9**, 2682–2696 (2015).
18. Shanks, A. L. & Reeder, M. L. Reducing microzones and sulfide production in marine snow. *Mar. Ecol. Prog. Ser.* **96**, 43–47 (1993).
19. Waeles, M., Maguer, J.-F., Baurand, F. & Riso, R. D. Off Congo waters (Angola Basin, Atlantic Ocean): a hot spot for cadmium-phosphate fractionation. *Limnol. Oceanogr.* **58**, 1481–1490 (2013).
20. Janssen, D. J. et al. Undocumented water column sink for cadmium in open ocean oxygen-deficient zones. *Proc. Natl Acad. Sci. USA* **111**, 6888–6893 (2014).
21. Simon, M., Grossart, H.-P., Schweitzer, B. & Ploug, H. Microbial ecology of organic aggregates in aquatic ecosystems. *Aquat. Microb. Ecol.* **28**, 175–211 (2002).
22. Burd, A. B. & Jackson, G. A. Particle aggregation. *Annu. Rev. Mar. Sci.* **1**, 65–90 (2009).
23. Lam, P. J. & Marchal, O. Insights into particle cycling from thorium and particle data. *Annu. Rev. Mar. Sci.* **7**, 159–184 (2015).
24. McDonnell, A., Boyd, P. & Buesseler, K. Effects of sinking velocities and microbial respiration rates on the attenuation of particulate carbon fluxes through the mesopelagic zone. *Glob. Biogeochem. Cycles* **29**, 175–193 (2015).
25. Smayda, T. J. Normal and accelerated sinking of phytoplankton in the sea. *Mar. Geol.* **11**, 105–122 (1971).
26. Jin, Q. & Bethke, C. M. Predicting the rate of microbial respiration in geochemical environments. *Geochim. Cosmochim. Acta* **69**, 1133–1143 (2005).
27. Guidi, L. et al. Relationship between particle size distribution and flux in the mesopelagic zone. *Deep Sea Res. Pt I* **55**, 1364–1374 (2008).
28. Durkin, C. A., Estapa, M. L. & Buesseler, K. O. Observations of carbon export by small sinking particles in the upper mesopelagic. *Mar. Chem.* **175**, 72–81 (2015).
29. Ploug, H., Iversen, M. & Fischer, G. Ballast, sinking velocity and apparent diffusivity in marine snow and zooplankton fecal pellets: implications for substrate turnover by attached bacteria. *Limnol. Oceanogr.* **53**, 1878–1886 (2008).
30. Picheral, M. et al. The Underwater Vision Profiler 5: an advanced instrument for high spatial resolution studies of particle size spectra and zooplankton. *Limnol. Oceanogr. Methods* **8**, 462–473 (2010).
31. Weber, T., Cram, J. A., Leung, S. W., DeVries, T. & Deutsch, C. Deep ocean nutrients imply large latitudinal variation in particle transfer efficiency. *Proc. Natl Acad. Sci. USA* **113**, 8606–8611 (2016).
32. Kalvelage, T. et al. Aerobic microbial respiration in oceanic oxygen minimum zones. *PLoS ONE* **10**, e0133526 (2015).
33. Johnston, D. et al. Placing an upper limit on cryptic marine sulphur cycling. *Nature* **513**, 530–533 (2014).
34. Martin, J. H., Knauer, G. A., Karl, D. M. & Broenkow, W. W. VERTEX: carbon cycling in the northeast Pacific. *Deep Sea Res. Pt A* **34**, 267–285 (1987).
35. Ohnemus, D. C. et al. Elevated trace metal content of prokaryotic communities associated with marine oxygen deficient zones. *Limnol. Oceanogr.* **62**, 3–25 (2017).
36. Lee, J.-M., Heller, M. I. & Lam, P. J. Size distribution of particulate trace elements in the US GEOTRACES Eastern Pacific Zonal Transect (GP16). *Mar. Chem.* (in the press).
37. Guidi, L. et al. Plankton networks driving carbon export in the oligotrophic ocean. *Nature* **532**, 465–470 (2016).
38. DeVries, T., Deutsch, C., Primeau, F., Chang, B. & Devol, A. Global rates of water-column denitrification derived from nitrogen gas measurements. *Nat. Geosci.* **5**, 547–550 (2012).
39. Deutsch, C., Gruber, N., Key, R. M., Sarmiento, J. L. & Ganachaud, A. Denitrification and N_2 fixation in the Pacific Ocean. *Glob. Biogeochem. Cycles* **15**, 483–506 (2001).
40. Bianchi, D., Dunne, J. P., Sarmiento, J. L. & Galbraith, E. D. Data-based estimates of suboxia,denitrification, and N_2O production in the ocean and their sensitivities to dissolved O_2. *Glob. Biogeochem. Cycles* **26**, GB2009 (2012).
41. Elderfield, H. & Rickaby, R. Oceanic Cd/P ratio and nutrient utilization in the glacial Southern Ocean. *Nature* **405**, 305–310 (2000).
42. Franck, V. M., Bruland, K. W., Hutchins, D. A. & Brzezinski, M. A. Iron and zinc effects on silicic acid and nitrate uptake kinetics in three high-nutrient, low-chlorophyll (HNLC) regions. *Mar. Ecol. Progress. Ser.* **252**, 15–33 (2003).
43. Brandes, J. A. & Devol, A. H. A global marine-fixed nitrogen isotopic budget: implications for Holocene nitrogen cycling. *Glob. Biogeochem. Cycles* **16**, 1120 (2002).
44. Deutsch, C., Sigman, D. M., Thunell, R. C., Meckler, A. N. & Haug, G. H. Isotopic constraints on glacial/interglacial changes in the oceanic nitrogen budget. *Glob. Biogeochem. Cycles* **18**, GB4012 (2004).
45. DeVries, T., Deutsch, C., Rafter, P. & Primeau, F. Marine denitrification rates determined from a global 3-D inverse model. *Biogeosciences* **10**, 2481–2496 (2013).
46. Großkopf, T. et al. Doubling of marine dinitrogen-fixation rates based on direct measurements. *Nature* **488**, 361–364 (2012).
47. Halm, H. et al. Heterotrophic organisms dominate nitrogen fixation in the South Pacific Gyre. *ISME J.* **6**, 1238–1249 (2012).
48. Bopp, L. et al. Multiple stressors of ocean ecosystems in the 21st century: projections with CMIP5 models. *Biogeosciences* **10**, 6225–6245 (2013).
49. Deutsch, C. et al. Centennial changes in North Pacific anoxia linked to tropical trade winds. *Science* **345**, 665–668 (2014).

Acknowledgements

D.B. was supported by NSF grant OCE-1635632; T.S.W. was supported by NSF grant OCE-1635414; C.D. was supported by the Gordon and Betty Moore Foundation (GBMF 3775); and R.K. was supported by the German Science Foundation through the Collaborative Research Center 754 'Climate-Biogeochemistry Interactions in the Tropical Ocean'. We thank D. Janssen and S. John for providing trace metal data from the Mauritanian region. We further acknowledge J. Coindat and S. Fevre of Hydroptic, and L. Stemman and M. Picheral for support during work with the UVP5.

Author contributions

D.B. and T.S.W. conceived the project, developed the microenvironment and particle models, conducted the simulations and analysed output, with contributions from C.D. R.K. provided UVP5 particle observations and suggested their use for model validation. D.B. and T.S.W. wrote the paper, with contributions from C.D. and R.K.

Competing interests

The authors declare no competing interests.

Additional information

Supplementary information is available for this paper at https://doi.org/10.1038/s41561-018-0081-0.

Reprints and permissions information is available at www.nature.com/reprints.

Correspondence and requests for materials should be addressed to D.B.

Publisher's note: Springer Nature remains neutral with regard to jurisdictional claims in published maps and institutional affiliations.

Methods

Overview of the particle microenvironment model. We expanded on previous work[15,50] to develop a size-resolved model of particle sinking and remineralization that also includes chemical processes at the particle scale (Fig. 1).

The model tracks the number, organic carbon mass and Cd content of a size spectrum of particles as they sink out of the euphotic zone and remineralize through a one-dimensional (1D) water column (Fig. 1a). Depending on particle size and seawater chemistry, O_2 (the default oxidant) can be exhausted inside particles creating zones where NO_3^- and SO_4^{2-} are utilized for organic matter respiration (Fig. 1b,c). For each particle size class and depth level, the model calculates the fraction of particle volume where respiration is fuelled by O_2, NO_3^- and SO_4^{2-}, and converts these into carbon respiration and oxidant utilization rates. The model further tracks the Cd content of each particle by allowing cadmium sulfide (CdS) to precipitate when SO_4^{2-} reduction takes place, and CdS dissolution when particles return to oxygenated conditions.

We implemented the 1D water column model for the Mauritanian[20] and Peruvian[11] upwelling systems (Fig. 2 and Supplementary Fig. 2), constraining the model with particle size spectra observations from underwater vision profilers. We then extended model predictions globally by conducting a 1D calculation at each latitude and longitude using climatological O_2 and NO_3^- as boundary conditions (Fig. 4), and propagated the uncertainty from model parameters and particle export estimates.

The model formulation and implementation are described in the following Methods sections; detailed derivations, model equations and numerical methods are presented in the Supplementary Information.

Particle size spectrum model. We expanded an existing particle size spectrum model (PRiSM)[50], and re-calibrated it with UVP5 observations[27,30]. The model tracks the POC mass of a size spectrum of particles, characterized by their radius r_0, as they sink through the water column. The size distribution n (number per volume per size increment) of particles evolves below the euphotic zone (z_{eu}) and is determined by the following equation:

$$\frac{\partial n}{\partial t} = \frac{\partial (w_s n)}{\partial z} + \frac{\partial}{\partial r_0}\left(\frac{\partial r_0}{\partial t} n\right) + C + F \qquad (1)$$

solved for steady state $\left(\frac{\partial n}{\partial t} = 0\right)$. The first two terms on the right-hand side of equation (1) represent gravitational settling and the change in particle size due to remineralization respectively, and have been previously described[50]. Briefly, particles sink at a speed $w_s = c_w r_0^\eta$, where c_w is a reference velocity coefficient and η the allometric exponent[25,51]. We do not attempt to resolve poorly understood processes of particle colonization by heterotrophs, but instead assume that aggregates are internally colonized by microbes with a range of metabolic capabilities, which maintain uniform remineralization rates throughout the particles. Remineralization is represented by first-order mass loss at rate c_r, so that $\frac{\partial \mathrm{POC}}{\partial t} = -c_r \mathrm{POC}$ following an individual particle. The POC mass is described by the empirically derived power law $\mathrm{POC} = c_m\ r_0^\alpha$, where c_m is a reference carbon content, and α an allometric exponent that encapsulates the fractal nature of marine particles[14,27]. It follows that $\frac{\partial c_m r_0^\alpha}{\partial t} = -c_r c_m r_0^\alpha$, which can be recast to yield the equation for the particle radius rate of change $\frac{\partial r_0}{\partial t} = -\frac{c_r}{\alpha} r_0$ in equation (1). The boundary condition for equation (1) is the initial particle spectrum leaving the base of the euphotic zone, which is assumed to follow a power-law relation $n(z = z_{eu}, r) = n_0 r^{-\beta_0}$, where n_0 determines the total number of particles, and the exponent β_0 the size distribution. A larger value of β_0 (that is, a 'steeper' spectrum) reflects a greater contribution of smaller particles.

Here, we extend the size spectrum model in two important ways. First, the original version neglected the effects of aggregation and disaggregation (C and F in equation (1) respectively), resulting in the preferential loss of small particles over depth that is not observed in size spectra profiles[27]. Because disaggregation rates exceed aggregation by up to an order of magnitude in subsurface waters[23], we include a term representing net disaggregation that converts large particles into a spectrum of smaller particles at a first-order rate (Supplementary Information Section 1.1). This simple approach does not resolve the poorly known processes of particle fragmentation, but ensures that the simulated size spectra remain close to observations. Second, we prescribe a decrease in c_r with depth, which more faithfully reproduces observed flux profiles in particle models[52]. The slowing of respiration at depth might be caused by a combination of different processes, including preferential remineralization of labile components and temperature effects. Again, we do not attempt to resolve the underlying mechanisms, and instead apply an empirical relationship for $c_r(z)$ derived from RESPIRE particle incubators[24] (Supplementary Information Section 1.2). The goal of this formulation is to reproduce a realistic size distribution and abundance of particles to integrate microenvironment processes, rather than exploring the details of particle transformations, which depend on a range of processes that are still poorly understood[53]. Additionally, POC decomposition rates (c_r) are slowed in our version when particles undergo anaerobic respiration (see below), by a factor (ε) proportional to the free energy yield of the metabolic pathway, compatible with theoretical considerations[26] and previous modelling studies[54] (Supplementary Tables 1 and 3).

Particle-scale microenvironments. In our model, microenvironments are represented as concentric shells inside a spherical particle, in which respiration is fuelled sequentially by O_2, NO_3^- and SO_4^{2-}, in the order of their energy yield[2] (Fig. 1b, c). We determine the volume of each microenvironment by calculating the denitrification radius, r_d, and the sulfidic radius, r_s (Fig. 1b,c), which mark the onset of denitrification and sulfate reduction respectively. Following previous work[15], we determine these radii by solving a spherical one-dimensional diffusion-reaction balance for the steady-state internal concentration of an oxidant X (O_2, NO_3^- or SO_4^{2-}) at distance r from the particle centre:

$$\frac{\partial^2 [X]}{\partial r^2} + \frac{2}{r}\frac{\partial [X]}{\partial r} - \frac{S_X}{D_p} = 0 \qquad (2)$$

Here, D_p is the diffusivity inside the particle and S_X is the volumetric sink of the oxidant X due to microbial respiration, which depends on the POC respiration rate and stoichiometry of the pathway. Equation (2) is solved for each particle size class at each depth, assuming diffusive equilibrium with the surrounding water column, to yield the anoxic radii r_d and r_s (Supplementary Information Sections 1.3–1.4). These radii are then used to subdivide the spherical particle volume into oxic, denitrifying and sulfidic fractions, and to partition total carbon remineralization rates into oxygen consumption, nitrate reduction and sulfate reduction rates. Figure 1c illustrates the internal concentrations of O_2, NO_3^- and SO_4^{2-} resulting from solution of the diffusion-reaction model.

Unresolved details of particle colonization by microbes, in combination with aggregation/disaggregation, could affect microenvironment dynamics. Fragmentation reduces particle sizes and exposes microenvironments to seawater. Under the model assumptions of uniform respiration and rapid equilibration with seawater (Supplementary Information Section 1.3), disaggregation leads to an overall reduction of microenvironment volumes.

Particle cadmium cycling. We track the Cd content of each model particle to test the hypothesis that CdS precipitation explains the Cd enrichment in particles from the Mauritanian upwelling zone[20]. Following an individual particle, CdS accumulation is tracked by the continuity equation:

$$\frac{d(\mathrm{CdS})}{dt} = J_{\mathrm{prec,CdS}} - k_s(\mathrm{CdS}) \qquad (3)$$

also solved for steady state. The first term on the right-hand side of equation (3) represents the precipitation rate of CdS in sulfidic particles (where r_s is greater than zero), and the second term represents a first-order dissolution rate of CdS, with a specific rate constant k_s, whenever sulfate reduction is not present. We assume that enough sulfide is produced in sulfidic particles to precipitate all Cd diffusing in from the seawater and released internally during remineralization. $J_{\mathrm{prec,CdS}}$ can therefore be recast as the sum of a diffusive supply rate, and the organic Cd remineralization rate that is assumed to be proportional to POC remineralization. See Supplementary Information Section 1.5 for equations.

Model parameterizations and observational constraints. Our model represents all particles between a radius of 10 μm and a radius of 2.5 mm, corresponding to the approximately log-linear portion of the size spectra detected by UVP5[27,30], and within the range where diffusive balance applies for sinking particles[55].

Particle parameters were derived from direct observations wherever possible. We used a metamodel approach to specify POC mass as a function of size, by compiling observed relationships from previous work, including two studies of plankton cells[56,57], four studies of large aggregates[58,59] and one study combining an underwater camera with measured carbon fluxes[60]. We fit an allometric power-law to these observations across the size spectrum of the model (Supplementary Fig. 1). We adopted an observed relationship between size and sinking velocity[25], and used it to estimate the thickness of the diffusive boundary layer δ_e surrounding the particle following previous work[55] (Supplementary Information Section 1.3). Based on laboratory incubations[29] we assumed that the diffusivity in particles (D_p) is 95% of the diffusivity in seawater (D_w). As lower diffusivities inside particles facilitate the exhaustion of oxidants, choosing particle diffusivities close to seawater leads to conservative estimates of microenvironment occurrence.

Case studies and optimization of model parameters. The 1D model was implemented in case studies of the ESTP and the Mauritanian upwelling zone (see Supplementary Information Section 1.7 for the details of the numerical implementation). In both regions, we combined particle counts from multiple UVP5 profiles to provide a robust characterization of the particle size spectrum that can be used to constrain the model (Supplementary Fig. 2b,d). The initial particle spectrum slope (β_0) was obtained by fitting a power-law equation to the composite profiles at 50 m, a typical z_{eu} for productive tropical regions[61]. We used observed profiles of $[O_2]$ and $[NO_3^-]$ as chemical boundary conditions for the diffusive calculations, and profiles of temperature and salinity to compute diffusivity and viscosity.

The attenuation of the POC flux over depth is determined by the mean particle sinking speed (~100 m day^{-1} averaged over all model particle sizes), and the particle remineralization rate. We selected parameters for $c_r(z)$ that are consistent with observations (Supplementary Fig. 1b) and yield 'Martin-like' flux profiles[34] (Supplementary Figs. 3–4), that is, where organic carbon flux (F) is approximated by $F=F_{(z=z_{\mathrm{eu}})}(z/z_{\mathrm{eu}})^{-b}$, with an attenuation parameter (b) close to 0.85 in oxic waters (anoxic water results in slower attenuation, due to curtailing of respiration once sulfate reducing conditions are reached).

The rate of particle disaggregation is a free parameter that we tuned separately at each site to ensure that the model reproduces the observed composite size spectra over depth. At both sites, the model faithfully reproduces the observed size spectra, whereas the original PRiSM that neglects disaggregation does not (Supplementary Figs. 3–4). We find that a faster disaggregation rate is required in the Mauritanian upwelling zone than in ETSP, but in both regions disaggregation rates lie comfortably within the observed range in a recent compilation[23].

To determine if the particle composition observed at GEOTRACES site USGT 10-09[20] is consistent with the mechanism of CdS precipitation, we tested whether our model can reproduce observed profiles of particulate Cd and Cd:P without violating observational constraints on the model parameters. Particulate P is assumed to be proportional to POC, and particulate Cd is the sum of CdS (equation (3)) and organic Cd (again proportional to POC). Four model parameters (c_{m}, c_r^{opt}, c_r^{min}, k_{s}) were optimized within observed ranges (Supplementary Table 4) to best match these profiles (Supplementary Information Section 1.8), which did not require significant deviations from their default values.

Global implementation. To estimate the global distribution of anaerobic microenvironments and the metabolic rates they harbour, we repeated the 1D model calculations using each profile of [O_2], [NO_3^-], temperature and salinity in the World Ocean Atlas 2009 database[62] as inputs. We assumed a spatially uniform surface size spectrum slope for these calculations ($\beta_0=3.5$), based on a global database of UVP5 observations[37] (Supplementary Fig. 7). This may lead to regional biases, but we estimated these to be of minor importance (Supplementary Information Section 2). Other model parameters were set at the default values in Supplementary Table 3, apart from c_{m}, c_r^{opt} and c_r^{min}. Relatively broad uncertainty ranges have been established for these parameters based on numerous observations (Supplementary Fig. 1), and we propagated this uncertainty into our global results by repeating the calculation with a broad swathe of parameter choices (24 combinations, Supplementary Table 4). We note that further uncertainties might arise from other poorly constrained parameters, such as the relative efficiency of aerobic and anaerobic respiration (ε values, see discussion in Supplementary Section 1.6), but these cannot be adequately quantified without further observational constraints.

Integrating across the size spectrum (as in Fig. 2c,f), these calculations yield the contribution of denitrifying and sulfate reducing microenvironments to total particle volume and respiration at 1° × 1° horizontal resolution, and over 33 vertical levels. These contributions were then integrated over depth and averaged across the 24 simulations with different parameter sets to obtain the 2D maps shown in Fig. 4. To convert to absolute rates of each respiration pathway, these 'fractional contribution' results were combined with independent estimates of POC export from the euphotic zone. Uncertainties in POC export and model parameters were propagated into these rates, by combining each of the 24 model simulations with nine different satellite-derived C export estimates (three algorithms for net primary production[63–65] and three algorithms for the carbon export ratio[66–68]). This yielded 216 different denitrification estimates, from which we report the mean and standard deviation as an estimate of uncertainty (Fig. 4c).

We also estimated global precipitation rates of the chalcophile trace metals Cd and Zn into sulfidic microenvironments (equation (3)). Although Cd and Zn observations are still too sparse to objectively map their global distributions, these metals correlate strongly with phosphate and silicic acid respectively[69,70]. We applied these correlations to the World Ocean Atlas 2009 phosphate and silicic acid fields to produce synthetic global distributions of Cd and Zn to use as boundary conditions in the particle diffusive model.

Sensitivity to climate-driven oxygen variations. To illustrate the different sensitivities of tropical and extratropical denitrification to climate change, we forced the global particle model with multimodel mean [O_2] changes from five simulations from the CMIP5 ensemble (see Supplementary Table 5 for a list of the models) under the RCP8.5 high-emission scenario[48]. This [O_2] change is the difference between year 2100 and year 1900, averaged for the five models (Fig. 5a), and is imposed as a perturbation to the climatological [O_2]. All other aspects of the model are kept constant to present-day climatological values. Thus, changes in denitrification from this simulation (Fig. 5b) only reflect changes in O_2 driven by climate change, and do not include changes in temperature, circulation, nutrient distribution, productivity, particle export and other environmental parameters[48].

Data availability. The data that support the findings of this study are available from the authors upon request. UVP5 observations from the Tara expedition are available at https://doi.pangaea.de/10.1594/PANGAEA.836321. Particle data from the Peruvian and Mauritanian upwelling are available at https://doi.pangaea.de/10.1594/PANGAEA.885760. Gridded temperature, salinity, nitrate and oxygen from the World Ocean Atlas are available from the NOAA National Centers for Environmental Information (https://www.nodc.noaa.gov/OC5/indprod.html). Net Primary Production data used to estimate POC export is available from http://www.science.oregonstate.edu/ocean.productivity/index.php. CMIP5 model output is available via the Earth System Grid data portal (http://pcmdi9.llnl.gov/).

Code availability. The code of the particle microenvironment model is available in the Supplementary Information. The code of the one-dimensional particle size-spectrum model is available from the authors upon request.

References

50. DeVries, T., Liang, J.-H. & Deutsch, C. A mechanistic particle flux model applied to the oceanic phosphorus cycle. *Biogeosciences* **11**, 5381–5398 (2014).
51. Stemmann, L. et al. Volume distribution for particles between 3.5 to 2000 μm in the upper 200m region of the South Pacific Gyre. *Biogeosciences* **5**, 299–310 (2008).
52. Jokulsdottir, T. & Archer, D. A stochastic, Lagrangian model of sinking biogenic aggregates in the ocean (SLAMS 1.0): model formulation, validation and sensitivity. *Geosci. Model Dev.* **9**, 1455–1476 (2016).
53. Passow, U. & Carlson, C. A. The biological pump in a high CO_2 world. *Mar. Ecol. Progress. Ser.* **470**, 249–271 (2012).
54. Louca, S. et al. Integrating biogeochemistry with multiomic sequence information in a model oxygen minimum zone. *Proc. Natl Acad. Sci. USA* **113**, E5925–E5933 (2016).
55. Ploug, H., Hietanen, S. & Kuparinen, J. Diffusion and advection within and around sinking, porous diatom aggregates. *Limnol. Oceanogr.* **47**, 1129–1136 (2002).
56. Litchman, E., Klausmeier, C. A., Schofield, O. M. & Falkowski, P. G. The role of functional traits and trade-offs in structuring phytoplankton communities: scaling from cellular to ecosystem level. *Ecol. Lett.* **10**, 1170–1181 (2007).
57. Mullin, M., Sloan, P. & Eppley, R. Relationship between carbon content, cell volume, and area in phytoplankton. *Limnol. Oceanogr.* **11**, 307–311 (1966).
58. Alldredge, A. The carbon, nitrogen and mass content of marine snow as a function of aggregate size. *Deep Sea Res. Pt I* **45**, 529–541 (1998).
59. Ploug, H. & Grossart, H.-P. Bacterial growth and grazing on diatom aggregates: respiratory carbon turnover as a function of aggregate size and sinking velocity. *Limnol. Oceanogr.* **45**, 1467–1475 (2000).
60. Iversen, M. H., Nowald, N., Ploug, H., Jackson, G. A. & Fischer, G. High resolution profiles of vertical particulate organic matter export off Cape Blanc, Mauritania: degradation processes and ballasting effects. *Deep Sea Res. Pt I* **57**, 771–784 (2010).
61. Lee, Z. et al. Euphotic zone depth: its derivation and implication to ocean-color remote sensing. *J. Geophys. Res. Oceans* **112**, C03009 (2007).
62. Garcia, H. et al. *World Ocean Atlas 2009, Volume 3: Dissolved Oxygen, Apparent Oxygen Utilization, and Oxygen Saturation* NOAA Atlas NESDIS 70 (U.S. Government Printing Office, Washington, DC, 2010).
63. Behrenfeld, M. J. & Falkowski, P. G. Photosynthetic rates derived from satellite-based chlorophyll concentration. *Limnol. Oceanogr.* **42**, 1–20 (1997).
64. Carr, M.-E. et al. A comparison of global estimates of marine primary production from ocean color. *Deep Sea Res. Pt II* **53**, 741–770 (2006).
65. Behrenfeld, M. J., Boss, E., Siegel, D. A. & Shea, D. M. Carbon-based ocean productivity and phytoplankton physiology from space. *Glob. Biogeochem. Cycles* **19**, GB1006 (2005).
66. Dunne, J. P., Armstrong, R. A., Gnanadesikan, A. & Sarmiento, J. L. Empirical and mechanistic models for the particle export ratio. *Glob. Biogeochem. Cycles* **19**, GB4026 (2005).
67. Laws, E. A., Falkowski, P. G., Smith, W. O., Ducklow, H. & McCarthy, J. J. Temperature effects on export production in the open ocean. *Glob. Biogeochem. Cycles* **14**, 1231–1246 (2000).
68. Laws, E. A., D'Sa, E. & Naik, P. Simple equations to estimate ratios of new or export production to total production from satellite-derived estimates of sea surface temperature and primary production. *Limnol. Oceanogr. Methods* **9**, 593–601 (2011).
69. de Baar, H. J., Saager, P. M., Nolting, R. F. & van der Meer, J. Cadmium versus phosphate in the world ocean. *Mar. Chem.* **46**, 261–281 (1994).
70. Wyatt, N. et al. Biogeochemical cycling of dissolved zinc along the GEOTRACES South Atlantic transect GA10 at 40S. *Glob. Biogeochem. Cycles* **28**, 44–56 (2014).